SMAR 2017 – Fourth Conference on Smart Monitoring,
Assessment and Rehabilitation of Civil Structures

SMAR 2017

Stress-strain Response of Steel-FRP Confined Concrete Columns Determined by DIC

Christian Carloni[1], Mattia Santandrea[1], Faezeh Ravazdezh[1], and Lesley Sneed[2]

[1] Department of Civil, Chemical, Environmental, and Materials Engineering, University of Bologna, Viale Risorgimento 2, 40126, Bologna, Italy
[2] Missouri University of Science and Technology, Rolla, Missouri, USA

ABSTRACT: Fiber-reinforced polymer (FRP) composites are comprised of continuous fibers embedded in a thermosetting resin. The use of externally bonded FRP sheets is a well-established technique for strengthening and rehabilitation applications of existing concrete structures. FRP provides several advantages when compared with traditional strengthening systems. Steel-FRP composites, also known as steel reinforced polymer (SRP) composites, are a suitable strengthening system due to the high strength and the low cost of steel fibers. In this study, the stress-strain response of axially unreinforced concrete columns subjected to concentric load and confined by steel-FRP composites is investigated. An experimental study is carried out to understand the behavior of short concrete prisms with a square cross-section confined by steel-FRP. The effectiveness of the confinement is studied in terms of peak stress with respect to unconfined (control) prisms. Test variables considered in this study are the density of steel fibers, concrete corner condition, concrete surface treatment, and number of confinement layers. Digital image correlation (DIC) is used to obtain the strain field on the surface of one face of the column during the test. Axial strain values determined by DIC are in good agreement with those determined from LVDT measurements.

1 INTRODUCTION

Fiber-reinforced composites have recently achieved a wide usage for strengthening and rehabilitation of existing concrete structures. Recent seismic events that occurred in several European countries (e.g. Italy, Greece, and Turkey) emphasize the importance of satisfying the beam-column hierarchical relationship in the design of beams and columns in a frame subjected to seismic loading. The confinement of concrete columns with composite materials can successfully improve the load-bearing capacity and deformability of the structural member, as shown by Saafi et al. (1999) and Rochette et al. (2000).

In the last decades, fiber reinforced polymer (FRP) composites achieved a resounding success in the field of strengthening applications due to several advantages such as ease of installation, high to strength-to-weight ratio, and good corrosion resistance. Recently steel-FRP or steel reinforced polymer (SRP) composite, which employs steel cords as fibers, has entered the market of strengthening systems. The low cost of the steel fibers compared to carbon or aramid fibers makes steel-FRP a competitive composite material. The available literature is focused on the use of steel-FRP composites for flexural strengthening of reinforced concrete (RC) beams (Wobbe et al. 2004, Prota et al. 2004, Kim et al. 2005, Pecce et al. 2006, Hawileh et al. 2014) and RC slabs (Napoli et al. 2015), and confinement of concrete columns (El-Hacha et al. 2012, Napoli et al. 2016).

In this work, the stress-strain response of concrete compressive members confined by steel-FRP composites is investigated. An experimental study is carried out to understand the behavior of short concrete prisms with a square cross-section confined by steel fiber sheets embedded in an epoxy matrix. Peak stress of unconfined and confined columns are reported and compared. The density of steel fibers, concrete corner condition, concrete surface treatment, and number of confinement layers are varied. Digital image correlation (DIC) is used to compute the strain field on the surface of the composite during the test.

2 EXPERIMENTAL PROGRAM

2.1 Materials

Concrete columns were cast using normalweight concrete with portland cement and a maximum aggregate size of 15 mm. The same batch of concrete was used to cast all columns of the experimental campaign. Additional prisms, cubes, and cylinders employed to fully characterize concrete were cast within the same batch. Compressive and tensile strengths of concrete were measured at 21 (compression only), 28, 42, 56, 84, 112, 168, 224, and 420 days after casting using 150 mm side cubes (compression) and 150 mm × 300 mm cylinders (splitting) tested according to EN 12390-3 and EN 12390-6, respectively. The average values of three tests for each day are plotted in Figure 1. Unconfined and confined columns were tested within the time range marked in Figure 1 with a grey area.

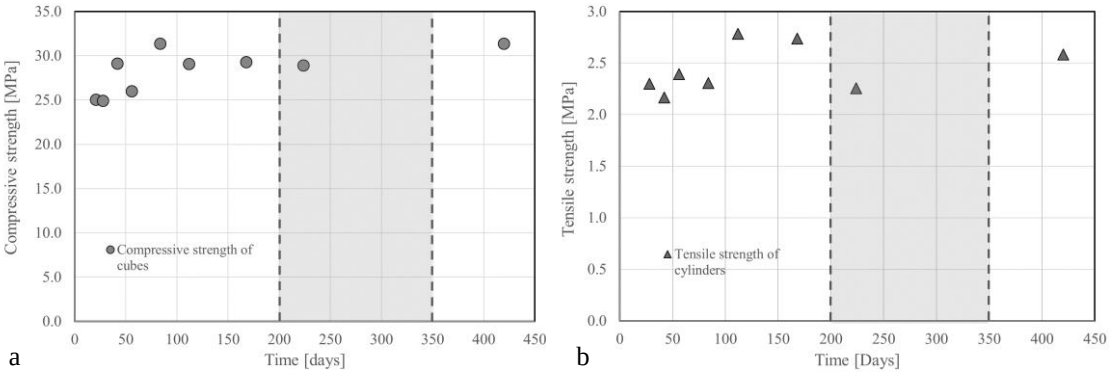

Figure 1. Concrete strength gain: a) compressive strength, b) tensile strength.

The classical three point bending set-up of a notched concrete prism was used to determine the fracture energy of concrete. Two sizes of the prism were considered. Three prisms were 600 mm length × 150 mm width × 150 mm depth, and three prisms were 300 mm length × 75 mm width × 75 mm depth. Further details about the fracture mechanics set-up and specimen preparation are reported in Santandrea et al. (2017). The fracture energy, G_F, was determined from the work of fracture as originally proposed by Hillerborg (1985) (see also Elices et al. (1992) and Hoover et al. (2013)). The fracture energy, G_F, was determined to be equal to 0.104 N/mm (CoV 0.05) and 0.109 N/mm (CoV 0.12) for the 600 mm × 150 mm × 150 mm prisms and the 300 mm × 75 mm × 75 mm prisms, respectively.

The composite material used to confine the short concrete columns consisted of steel fiber cords embedded in a polymeric matrix. Steel fibers (cords) were in the form of a unidirectional sheet made of ultra-high strength galvanized steel micro-cords fixed to a fiberglass micromesh to facilitate installation. Each micro-cord consisted of five filaments. Three of the five filaments were straight, and the remaining two filaments were wrapped around the other three with a high

torque angle. The cross-sectional area of the cord A_{cord} was equal to 0.538 mm^2. Two different fiber densities were studied and are referred to in this paper as medium density (MD) steel fibers and high density (HD) steel fibers. The MD steel fiber sheets had 0.314 cords/mm, and the HD steel fiber sheets had 0.472 cords/mm. Mechanical properties of the fibers are reported in Table 1 (Kerakoll 2017). The matrix was a two-component epoxy thixotropic gel system, whose mechanical properties are reported in Table 2 (Kerakoll 2017).

Table 1. Properties of steel fibers provided by manufacturer (Kerakoll 2017).

Steel fibers	Number of cords/mm	Tensile strength [MPa]	Elastic Modulus [GPa]	Break Deformation [%]	Equivalent thickness [mm]
Medium density (MD)	0.314	> 3000	> 190	> 2	≈ 0.168
High density (HD)	0.472	> 3000	> 190	> 2	≈ 0.254

Table 2. Mechanical properties of epoxy provided by manufacturer (Kerakoll 2017).

Matrix	Tensile strength	Flexural elastic modulus	Elastic modulus under compression
Epoxy	> 14 MPa	> 2.50 GPa	> 5.30 GPa

2.2 Specimen Description and Preparation

Twenty-three concrete prisms were tested under a concentric compressive loading condition. Eighteen concrete prisms out of the 23 were confined, while five were left unconfined and were used as control specimens. The nominal dimensions of the concrete prisms were width (b) = 150 mm × depth (h) = 150 mm × length (L) = 450 mm, with an aspect ratio equal to 3. All prisms were axially unreinforced. Specimens were named following the notation SQ-X-A-B-C-D-Y-Z, where SQ indicates a square cross-section, X indicates the confined length (h_c) in mm, i.e. the portion of the prism length wrapped with the composite material, A indicates the fiber density (MD = medium density, HD = high density), B indentifies the composite used in this study (UC = unconfined, CE = confined epoxy-based matrix), C denotes the concrete surface treatment (T = treated with sand-blasting, UT = untreated), D indicates the concrete corner condition (R = rounded to a radius r = 17.5 mm, S = sharp, i.e., r = 0), Y indicates the number of confinement layers (1L = one layer, 2L = two layers), and Z = specimen number. The unconfined specimens were named following the notation SQ-B-C-D-Z with the parameters B, C, D, and Z defined above. Specimens are listed in Table 3.

The confined columns were wrapped following the manufacturer's recommendations, and the wet lay-up procedure was used to apply the composite. Fibers were arranged in the hoop direction, i.e. perpendicular to the longitudinal axis of the column. The steel fiber sheets were pre-bent in order to conform to the surface. For the confined specimens with rounded corners, columns were chamfered with a grinder to obtain the designated corner radius prior to applying the composite. Since the width of the fiber sheet was not the same as the length of the prisms, the prisms were wrapped with two or three segments of the fiber sheet with no overlap of the different segments along the column length. On the other hand, as they were wrapped around the perimeter, fibers overlapped for a length equal to the width of one prism face. Confined prisms were left to cure in the laboratory for seven days after casting. Prior to testing, both ends of each prism were capped with a 4 mm thick layer of high strength mortar to ensure that the ends were flat and parallel to one another.

Three-dimensional (3-D) DIC was used to determine the displacement field and compute the strain field on one face (which will be referred to as the front face in this paper) of the confined prism. The front composite surface was painted white prior to testing. A speckle pattern was created by spraying black paint on the composite surface. The DIC software uses the variation of greys in the speckle pattern to track black dots and thus obtain the displacement field. Images were taken at a frequency of 0.1 Hz. Displacements were best fit by a quintic b-spline, and the strain components were then derived.

2.3 Test Procedure

The capacity of the compression testing machine was 4000 kN. Two linear variable displacement transducers (LVDTs) were mounted between the machine pressing plates at opposite corners to measure the relative displacement between the pressing plates, which was assumed as the shortening of the column. Tests were conducted by monotonically increasing the machine stroke in order to achieve a displacement rate of the average of the two LVDTs (named LVDT-a and LVDT-b) equal to 0.2 mm/min. The machine stroke was constantly monitored and adjusted to meet the target rate. Testing was stopped when a significant drop in load occurred in the post-peak response. Axial strains were determined by dividing the average of the displacement readings from LVDT-a and LVDT-b by the initial distance between the pressing plates. Two additional LVDTs, oriented in the direction of the column axis, were mounted directly to the specimen with bolts drilled into the concrete core (LVDT-c and LVDT-d in Figure 2b). The supports of LVDT-c and LVDT-d were placed at the third points along the column length.

a

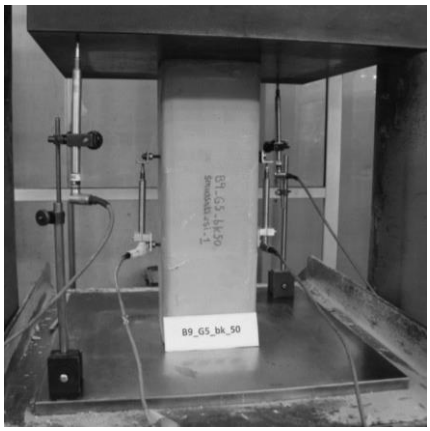

b

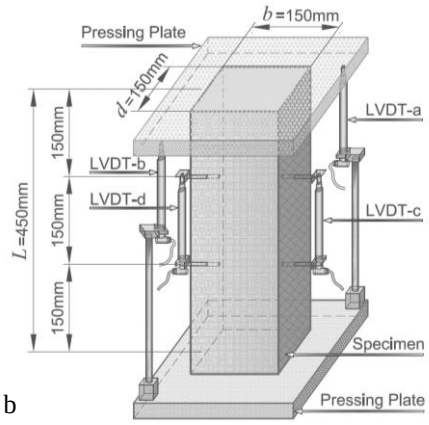

Figure 2. Test set-up: a) photo, b) sketch.

3 TEST RESULTS

The peak load of all concrete prisms was associated with crushing of concrete. After the peak load was achieved, the confined specimens continued to deform under decreasing applied load until failure occurred by separation of the steel-FRP jacket at the vertical lap joint. Fiber rupture was observed for specimens SQ-450-MD-CE-T-R-1L-1, SQ-450-MD-CE-T-S-1L-1, and SQ-450-MD-CE-T-S-1L-2. In these three specimens rupture of the fibers occurred before the composite opened where fibers overlapped. For most confined specimens, failure initiated near the middle third of the specimen length. Detachment of the overlapping layer of the jacket occurred along a limited portion of the specimen length. Cracks parallel to the fibers defined the portion of the FRP jacket that was completely opened. These cracks initiated on the face where

fibers overlapped and extended to adjacent faces of the specimen. It was not possible to determine where crack initiation occurred, i.e. in between the layers of fibers or at the epoxy-concrete interface. However, after the test it was concluded that both layers of fibers opened. The external layer detached from the internal layer, and the internal layer debonded from the concrete substrate. Concrete particles remained attached to the epoxy layer. The failure mode differs from the fiber rupture observed in confined columns strengthened with traditional FRP systems. FRP confined specimens with carbon or glass fibers usually experience rupture of the fibers near the corners of the specimen, due to the brittle nature of the fibers.

Table 3. Experimental results.

GROUP	SPECIMEN	f'_{co} or f'_{cc}	$f'_{co,u}$ or f'_{ccu}	$\frac{f'_{cc}}{f'_{co}}$	Average $\frac{f'_{cc}}{f'_{co}}$
CONTROL	SQ-UC-UT-S-1	28.9	13.6	/	/
	SQ-UC-UT-S-2	24.1	19.1	/	
	SQ-UC-UT-S-3	27.6	21.0	/	
	SQ-UC-UT-S-4	25.8	20.5	/	
	SQ-UC-UT-S-5	23.4	21.0	/	
GROUP 1	SQ-450-HD-CE-UT-R-1L-1	34.9	31.0	1.35	1.39
	SQ-450-HD-CE-UT-R-1L-2	35.8	31.4	1.38	
	SQ-450-HD-CE-UT-R-1L-3	37.3	31.1	1.44	
GROUP 2	SQ-450-HD-CE-UT-S-1L-1	38.2	34.0	1.47	1.50
	SQ-450-HD-CE-UT-S-1L-2	39.8	33.9	1.53	
	SQ-450-HD-CE-UT-S-1L-3	38.6	33.1	1.49	
	SQ-450-HD-CE-UT-S-1L-4	39.3	31.4	1.51	
GROUP 3	SQ-450-HD-CE-T-R-1L-1	37.4	30.3	1.44	1.46
	SQ-450-HD-CE-T-R-1L-2	37.8	32.1	1.46	
	SQ-450-HD-CE-T-R-1L-3	38.3	33.3	1.47	
GROUP 4	SQ-450-MD-CE-T-R-1L-1	36.6	24.4	1.41	1.40
	SQ-450-MD-CE-T-R-1L-2	35.5	27.5	1.37	
	SQ-450-MD-CE-T-R-1L-3	36.7	27.0	1.41	
GROUP 5	SQ-450-MD-CE-T-S-1L-1	33.4	22.5	1.29	1.31
	SQ-450-MD-CE-T-S-1L-2	34.8	24.0	1.34	
	SQ-450-MD-CE-T-S-1L-3	33.7	23.1	1.30	
GROUP 6	SQ-450-MD-CE-T-S-2L-1	38.3	37.6	1.48	1.45
	SQ-450-MD-CE-T-S-2L-1	36.9	37.1	1.42	

All specimens were sawcut near the midlength to observe the crushing mechanism that occurred in the cross-section. The typical arch effect (Rochette et al. 2000) was observed. Photographs of a typical failed specimen are shown in Figure 3.

Table 3 summarizes the key experimental results obtained for each specimen. Values provided for the unconfined specimens include the unconfined compressive strength (peak stress) f'_{co} and the unconfined ultimate compressive stress $f'_{co,u}$. Values provided for the confined specimens include the confined compressive strength (peak stress) f'_{cc} and the confined ultimate compressive stress $f'_{cc,u}$. Values of the ultimate stress correspond to the stress at which a significant drop in load occurred in the post-peak load response and are associated with specimen failure. Values of stress were determined by dividing the force by the cross-sectional area of the prism (22,500 mm^2 and 22,237 mm^2 for specimens with sharp and rounded corners, respectively).

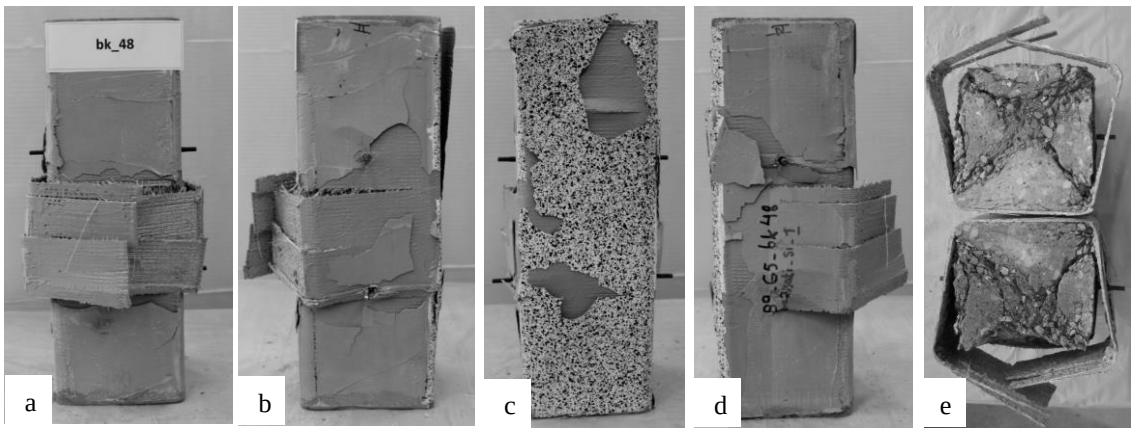

Figure 3. Failure mode of specimen SQ-450-HD-CE-T-R-1L-1: a) back face, b) left face, c) front face, d) right face, e) cut section.

4 DISCUSSION OF RESULTS

4.1 DIC analysis

DIC was used to examine the strain field on the surface of the composite in the axial and hoop (fiber) directions. DIC readings were recorded only until shortly after the peak load was achieved in order to protect the DIC equipment. Displacements and strains were obtained for different square areas (subsets) for a 5 pixel step size, which provide points spaced approximately 1.25 mm. Different subsets of 21, 31, and 41 pixels were used to study the influence of subset dimensions on the results obtained. Results determined using different subsets were similar; therefore a subset size of 31 pixels (approximately 3.40 mm) edge was employed (Figure 4a).

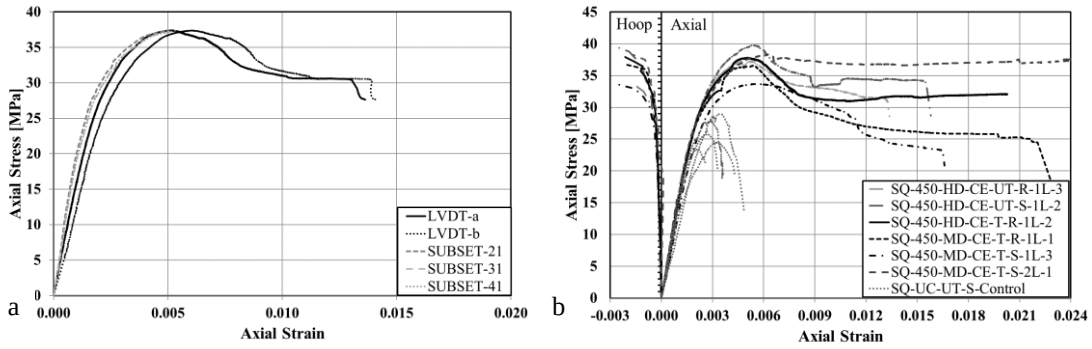

Figure 4. a) Comparison of axial stress – axial strain response determined by LVDTs and DIC (specimen SQ-450-HD-CE-T-R-1L-1), b) axial stress – hoop/axial strain response for representative specimens.

The strain values obtained by DIC and plotted in Figure 4a were evaluated analyzing strain values in eight squares in the central third of the specimen length. The squares had a 30 mm side. Adjacent squares were spaced 30 mm one another in the horizontal direction, while the vertical spacing was equal to 10 mm. The strain obtained by DIC was evaluated by averaging the strains within these eight squares. Figure 4a also shows the values of axial strain obtained from measurements by LVDT-a and LVDT-b. A similar behavior between strains evaluated by DIC and LVDTs (strain obtained from LVDT c and d was also similar but not reported for the sake of brevity) can be observed, therefore the strain values obtained from DIC can be considered reliable

and can be used to evaluate the hoop strains for specimens for which DIC was employed. Figure 4b shows the axial stress versus hoop strains (obtained from DIC) and axial strains (obtained from LVDTs) of representative specimens together with the axial stress-axial strain response of the control specimens. Values of hoop strain at peak stress were less than the ultimate strain (0.02) of the fibers for all specimens.

The contour plot of the out-of place displacement *w* of specimen SQ-450-HD-CE-T-R-1L-1 is shown in Figure 5 for different stress levels. DIC is able to capture the formation of the horizontal cracks and predict the opening of the steel FRP jacket.

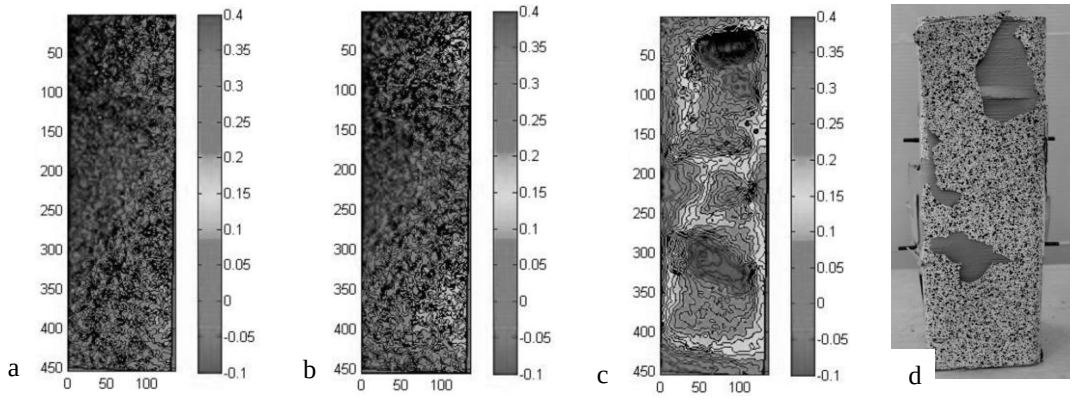

Figure 5. Out-of-plane displacements for specimen SQ-450-HD-CE-T-R-1L-1 at different values of the compressive stress: a) 26.2 MPa, b) 29.9 MPa, c) 37.4 MPa, d) failure mode.

4.2 Influence of test variables

Referring to the results presented in Table 3, the results of different groups of confined specimens are compared in this section to investigate the role that each parameter plays in the load-bearing capacity. The influence of corner condition is examined by comparing the results of specimens in Groups 1 and 2. Specimens with sharp corners consistently had higher compressive strength f'_{cc}, than those with corners rounded to a radius of 17.5 mm. The influence of concrete surface treatment is examined by comparing the results of Group 1 and 3. Specimens with a sandblasted surface had higher compressive strength than specimens with no treatment. Comparing the results of Groups 3 and 4, specimens reinforced with HD fibers had slightly higher compressive strength than specimens reinforced with MD fibers. The influence of the number of jacket layers is examined by comparing the results of specimens in Groups 5 and 6. Specimens with two layers had compressive strengths higher than those with one layer.

5 CONCLUSIONS

This paper presented results of an experimental study carried out to understand the behavior of short concrete prisms with a square cross-section confined by steel-FRP composite. The following conclusions can be made from the results:

- Axial strain values determined by DIC were found to be in good agreement with those determined by LVDT measurements.
- The confined compressive strength was found to be dependent on the corner condition, concrete surface treatment, fiber density, and number of jacket layers. Specimens with sharp corners had higher compressive strengths than those with rounded corners. The increase in the compressive strength for specimens with sharp corners is mainly due to

the failure observed, which was the result of detachment of the overlapping layer. Specimens with sharp corners achieved higher values of the load than specimens with rounded corners because they are able to delay the opening of the steel FRP jacket. Specimens with a sandblasted surface had higher compressive strengths than those with an untreated surface. Specimens with high density fibers had a slightly higher compressive strength than those with medium density fibers. Specimens with two layers of confinement had higher compressive strengths than those with one layer of confinement.

6 ACKNOWLEDGEMENTS

The experimental work presented in this paper was conducted in the laboratory of structural and geotechnical engineering (LISG) at the University of Bologna. Kerakoll spa, Sassuolo, Italy, is gratefully acknowledged for providing the composite materials.

7 REFERENCES

CEN, EN 12390-3, 2009. Testing hardened concrete - Part 3: Compressive strength of test specimens. A1: 2011. Brussels: CEN.

CEN, EN 12390-6, 2009. Testing hardened concrete - Part 6: Tensile splitting strength of test specimens.

El-Hacha, R., Mashrik, M.A. (2012). “Effect of SFRP Confinement on Circular and Square Concrete Columns.” Eng Struct, 36, 379-393.

Elices, M., Guinea, G. V., & Planas, J. (1992). “Measurement of the fracture energy using three-point bend tests: Part 3—influence of cutting the P-δ tail.” Materials and Structures, 25(6), 327-334.

Hawileh R., Abdalla J., Nawaz W., Alzeer A., Muwafi R., Faridi A. (2014). “Strengthening reinforced concrete beams in flexure using hardwire steel fiber sheets.” In: Proc. of CICE. Vancouver, Canada, August 20–22; p. 22.

Hillerborg, A. (1985). “The theoretical basis of a method to determine the fracture energy GF of concrete.” Materials and structures, 18(4), 291-296.

Hoover, C. G., & Bažant, Z. P. (2013). “Comprehensive concrete fracture tests: size effects of types 1 & 2, crack length effect and postpeak.” Engineering Fracture Mechanics, 110, 281-289.

Kerakoll S.p.A. – web site: <www.kerakoll.com> [accessed March 2017].

Kim J.Y., Fam A., Kong A., El-Hacha R. (2005). “Flexural strengthening of RC beams using steel reinforced polymer (SRP) composites.” In: Proc. of the 7th int. symp. FRP reinforcement for concrete structures, ACI SP-230, 1, Paper #93; 2005. p. 1647–64.

Napoli, A., Realfonzo, R. (2015). “Reinforced concrete beams strengthened with SRP/SRG systems: experimental investigation.” Const Build Mat; 93:654:677.

Napoli, A., Realfonzo, R. (2016). “Compressive Behavior of Concrete Confined by SRP Wraps.” Const Build Mat; http://dx.doi.org/10.1016/j.conbuildmat.2016.01.055

Pecce M., Ceroni F., Prota A., Manfredi G. (2006). “Response prediction of R/C beams externally bonded with steel reinforced polymers.” J Compos Constr; 103(2):195–203.

Prota A., Manfredi G., Nanni, A., Cosenza E., Pecce M. (2004). “Flexural strengthening of R/C beams using emerging materials: ultimate behavior.” In: Proc. of CICE. Adelaide, Australia; p. 163–70.

Rochette, P., Labossière, P. (2000). "Axial Testing of Rectangular Column Models Confined with Composites." J. Compos. Constr., 4(3), 129-136.

Saafi, M., Toutanji, H., Li, Z. (1999). “Behavior of Concrete Columns Confined with Fiber Reinforced Polymer Tubes.” ACI Mat J, 96(4), 500-509.

Santandrea, M., Carloni, C., & Wendner, R. “An investigation on the “width and size effect” in the evaluation of the fracture energy of concrete”. Procedia Structural Integrity. 3, 450-458.

Wobbe E., Silva P., Barton B.L., Dharani L.R., Birman V., Nanni A., Alkhrdaji T., Thomas J., Tunis T. (2004). “Flexural capacity of R/C beams externally bonded with SRP and SRG.” In: Proc. of society for the advancement of material and process engineering symp. Long Beach, CA, USA; p. 20–7.